Reanalysis of critical exponents for the $O(N)$ model via a hydrodynamic approach to the functional renormalization group

Fabrizio Murgana,[1,2,3,*] Adrian Koenigstein,[3,4,†] and Dirk H. Rischke[3,5,‡]

[1]*Department of Physics and Astronomy, University of Catania, Via Santa Sofia 64, I-95125 Catania, Italy*
[2]*INFN-Sezione di Catania, Via Santa Sofia 64, I-95123 Catania, Italy*
[3]*Institut für Theoretische Physik, Goethe-Universität, Max-von-Laue-Straße 1, D-60438 Frankfurt am Main, Germany*
[4]*Theoretisch-Physikalisches Institut, Friedrich-Schiller-Universität Jena, Max-Wien-Platz 1, D-07743 Jena, Germany*
[5]*Helmholtz Research Academy Hesse for FAIR, Campus Riedberg, Max-von-Laue-Straße 12, D-60438 Frankfurt am Main, Germany*

(Received 20 April 2023; revised 11 September 2023; accepted 27 November 2023; published 18 December 2023)

We reanalyze some critical exponents of the $O(N)$ model within the functional renormalization group (FRG) approach in the local potential approximation (LPA). We use recent advances which are based on the observation that the FRG flow equation in LPA can be put into the form of an advection-diffusion equation. This allows to employ well-tested hydrodynamical algorithms for its solution to better estimate various sources of errors. Our results complement previous results for the critical exponents obtained within the FRG approach in LPA and compare favorably with those obtained via other methods.

DOI: 10.1103/PhysRevD.108.116016

I. INTRODUCTION

Understanding the behavior of systems where the microscopic degrees of freedom are strongly interacting is the main goal of many areas of physics, ranging from condensed-matter [1,2] to elementary-particle theories [3,4], and extending even to quantum gravity [5,6]. However, first-principle calculations for these systems are often very difficult and demand powerful tools. Calculations are in particular challenging when a system undergoes a phase transition, since new degrees of freedom may arise and become relevant. In this case the underlying theory must consistently relate the two phases and thus describe the transition from one set of degrees of freedom to the other. For second-order transitions, the behavior of a system at all length scales is determined by a finite set of so-called critical exponents.

One out of many modern approaches to this problem is the functional renormalization group (FRG) [7–11], also referred to as exact renormalization group (RG) or nonperturbative RG, which is ultimately based on seminal ideas by Wilson [12–16] and others, see, e.g., Refs. [17,18]. The central object of the FRG approach is a flow equation which describes the evolution of correlation functions or, equivalently, their generating functional under the influence of fluctuations. It connects a well-defined initial quantity, e.g., the microscopic ultraviolet (UV) action, in an exact manner with the full infrared (IR) effective action, where all fluctuations are integrated out. Hence, solving the flow equation corresponds to solving the full theory and is therefore equivalent to a direct computation of the generating functional. Thanks to the fact that it is nonperturbative and connects degrees of freedom at different scales, the FRG approach is well-suited to address the issue of describing systems approaching criticality and phase transitions, and thus a tool for the computation of critical exponents, cf. Refs. [19–27].

Even though the FRG has a solid theoretical foundation, it is very hard to find analytical solutions to the flow equation. For specific problems, it can be converted into an infinite set of coupled partial differential equations (PDEs) and/or ordinary differential equations (ODEs), which, if suitably truncated, can be numerically solved. In fact, as a truncation scheme one often employs a derivative expansion of the effective action and solves separate FRG flow equations for the coefficients of this expansion. The leading-order truncation in this expansion only accounts for the flow of the local effective potential, and is thus called local potential approximation (LPA). Various numerical solution schemes have been proposed for this

*murgana@itp.uni-frankfurt.de
†adrian.koenigstein@uni-jena.de
‡drischke@itp.uni-frankfurt.de

PDE in the past. In this work, we briefly recapitulate some basics about the FRG approach in the LPA and its application to the $O(N)$ model, for which we recompute the critical exponents.

The critical exponents of the $O(N)$ model have already been studied within the FRG approach some time ago, see, e.g., Refs. [21,24,25,27,28]. The reason why we decided to repeat such an investigation is twofold. First, a novel method to solve the FRG flow equations has been recently proposed [29]. This already calls for repeating previous calculations and a comparison with established results to test the new framework. The novel approach relies on the observation that the FRG flow equation for the effective potential can be cast into the form of a hydrodynamic advection-diffusion equation. This suggests to use numerical techniques well-known from hydrodynamics to solve that equation, see also Refs. [30–36], as well as Refs. [37–43] for some early developments. In particular, hydrodynamic conservation laws in general allow for the formation of discontinuities or, more general, nonanalyticities in the solution. Therefore, the applied numerical scheme has to be able to handle discontinuities in an appropriate manner. While Ref. [29] used a discontinuous Galerkin method to solve the FRG flow equation, here we exploit a well-established finite-volume central scheme, the Kurganov-Tadmor (KT) algorithm, which is designed to have a high-order accuracy, preserving stability and introducing negligible dissipation, while allowing to treat discontinuities in the solution (see Ref. [44] for more details). Based on this, the second motivation for our investigation is to perform a more systematic study of various sources of errors in determining the critical exponents of the $O(N)$ model than previous attempts using the FRG approach in the LPA (without working with the fixed-point equations directly).[1] The reason behind this is that oftentimes literature results for critical exponents are only provided—if at all—with an overall error, while different contributions to this error, such as errors from numerical schemes, statistical errors, or fitting errors, are not resolved and discussed at all. This is not exclusive to the FRG method. In this work, we present estimates for the different contributions to the overall error and challenges in calculating them, which we believe to be relevant also for calculations in other truncation schemes.

This work is organized as follows. In Sec. II we give a brief introduction to the FRG approach and discuss the FRG flow equation. In Sec. III we provide the FRG flow equation for the $O(N)$ model in the LPA and rewrite it in the form of an advection-diffusion equation in order to solve it with the KT scheme. While most of the contents of Secs. II and III are well-known in the literature, we nevertheless decided to keep them in order to make the presentation as self-contained as possible. Numerical results for the critical exponents are presented in Sec. IV. A detailed discussion of error estimates is performed in Sec. V. Finally, we conclude this work in Sec. VI with a summary and an outlook.

[1]As already mentioned, there are more advanced truncations available for high-precision calculations of the critical exponents of $O(N)$ models via the FRG [24,25,27,28], and we do not attempt to compete with the respective results. However, since some of these works combine the use of fixed-point equations with the approach employed in this work, we believe that our results are still of sufficient interest to be published.

II. FUNCTIONAL RENORMALIZATION GROUP APPROACH

In this section, we briefly recapitulate the FRG approach in the formulation given by Wetterich *et al.* [45–48]. For further details, see Refs. [7–11]. The central object of this approach is the effective action $\Gamma[\Phi]$, which is the generating functional of 1PI vertex functions. In order to compute $\Gamma[\Phi]$, one introduces the so-called *effective average action* $\bar{\Gamma}_k[\Phi]$. This quantity depends on the parameter k, which is a coarse-graining scale with physical dimension of momentum. The FRG flow equation describes the evolution of $\bar{\Gamma}_k[\Phi]$ as k runs from the UV, $k \to \infty$, to the IR, $k \to 0$. The effective average action interpolates between the bare classical action $S_{\text{bare}}[\Phi]$ in the UV and the full quantum effective action $\Gamma[\Phi]$ in the IR, i.e.,

$$\bar{\Gamma}_{k\to\infty}[\Phi] = S_{\text{bare}}[\Phi], \qquad \bar{\Gamma}_{k\to 0}[\Phi] = \Gamma[\Phi]. \tag{1}$$

In practice, one may not always be able to send $k \to \infty$. Therefore, one usually introduces a UV scale Λ as initial scale for the FRG flow equation, which is chosen to be sufficiently large, i.e., much larger than any other physical scale of the theory, and assumes that the bare classical action describes the underlying theory at this scale. However, using a finite cutoff is an approximation and one has to ensure that the results are independent of the choice of Λ, e.g., by respecting RG consistency [49].

The equation that describes the RG-scale evolution of $\bar{\Gamma}_k[\Phi]$, i.e., how the effective average action varies as one integrates out fluctuations with increasingly smaller momenta, is the so-called *Wetterich equation*, or *exact renormalization group flow equation*, or simply *FRG flow equation* [45,50,51],

$$\partial_k \bar{\Gamma}_k[\Phi] = \mathrm{Tr}\left[\left(\tfrac{1}{2}\,\partial_k R_k\right)\left(\bar{\Gamma}_k^{(2)}[\Phi] + R_k\right)^{-1}\right] = \quad , \tag{2}$$

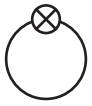

where the trace indicates an integral over momenta and a sum over all internal degrees of freedom. Here, the black line represents the full propagator $G_k[\Phi] = (\bar{\Gamma}_k^{(2)}[\Phi] + R_k)^{-1}$ and the crossed circle stands for $\frac{1}{2}\partial_k R_k$,

where R_k in Eq. (2) is the so-called *regulator*. The latter must be chosen such that $\bar{\Gamma}_k[\Phi]$ smoothly interpolates between the bare classical action $S_{\text{bare}}[\Phi]$ at $k = \Lambda$ and the full effective action $\Gamma[\Phi]$ at $k = 0$. This requirement imposes certain conditions on R_k. The choice of the specific shape of the regulator is a delicate issue and we refer to Refs. [52–55] for details.

Despite its deceptively simple form, the Wetterich equation is a functional integro-differential equation, and as such cannot be solved exactly for an arbitrary $\bar{\Gamma}_k[\Phi]$. Thus, it is clear that some approximation has to be made. Two common approximation schemes used in the literature are the vertex expansion [47,56] and the derivative expansion [11,57]. In this work we will focus on the latter, since the vertex expansion assumes regularity of $\bar{\Gamma}_k[\Phi]$, which is violated near phase transitions, where the effective action develops discontinuities or points of nonanalyticity during the FRG flow [29,30,34]. Since in this paper we are interested in critical exponents of second-order phase transitions, we have to employ a method which allows to treat discontinuities and nonanalyticities in the FRG flow of the effective action. The derivative expansion fulfills this requirement, even in the most simple truncation, the aforementioned LPA, which will be discussed in the next section.

III. APPLICATION: $O(N)$ MODEL IN LPA

In this section we will briefly introduce the $O(N)$ model and then apply the FRG approach in LPA to derive the respective flow equation.

A. The $O(N)$ model

Let us consider the $O(N)$ model in d-dimensional Euclidean space-time. The model describes the dynamics of N scalar fields $\phi_a(x)$, where $a = 1, \ldots, N$, with the bare action

$$S_{\text{bare}}[\vec{\phi}] = \int d^d x[(\partial_\mu \phi_a)^2 + V(\rho)], \tag{3}$$

where $V(\rho)$ is the potential parametrizing how the N scalar fields interact with each other. The $O(N)$ symmetry requires that $V(\rho)$ is solely a function of the variable

$$\rho = \frac{1}{2}\phi_a \phi_a, \tag{4}$$

where a sum over a from 1 to N is implied. Despite its apparent simplicity, the $O(N)$ model is used to describe a large variety of physical systems at different energy scales. For example, for $N = 4$ the model is commonly believed to describe the chiral phase transition in QCD with two quark flavors [58]. For $N = 3$ it belongs to the universality class of the Heisenberg model, describing a ferromagnetic phase transition [59]. The $N = 2$ case can be used to describe the XY model [60] and $N = 1$ belongs to the Ising universality class [61].

B. Derivation of the flow equation in LPA

In order to proceed with the quantitative study of the $O(N)$ model, the first step is to derive the flow equation that describes the k-evolution of the effective average action. As already mentioned in the previous section, we need to truncate the effective action, i.e., we need to choose an ansatz. We use the derivative expansion, expanding the effective action in terms of powers of gradients of the field. In particular we consider the lowest order of the expansion, the so-called LPA, where space-time derivatives of the fields appear only in the kinetic term and the effective potential $V(\rho)$ is solely a function of the fields but not of their space-time derivatives.

The advantage of the LPA is that it leads to a simple expression for the FRG flow equation, while still capturing many nontrivial features of the theory. Furthermore, this approximation becomes exact in the limit $N \to \infty$ [62]. In LPA the effective average action reads

$$\bar{\Gamma}_k[\vec{\varphi}] = \int \mathrm{d}^d x \left[\frac{1}{2}(\partial_\mu \varphi_a)^2 + V_k(\varrho)\right], \tag{5}$$

where $V_k(\varrho)$ is the effective potential which depends on the FRG scale parameter k and the $O(N)$-invariant $\varrho = \frac{1}{2}\varphi_a \varphi_a$, i.e., the quantity ρ defined in Eq. (4), evaluated for the mean fields φ_a. The next order in the derivative expansion would be the so-called LPA′, which considers nontrivial wave-function renormalization corrections, i.e., $(\partial_\mu \varphi_a)^2 \to Z_k(\partial_\mu \varphi_a)^2$, with Z_k being a nontrivial function of the FRG flow parameter k. For even better truncations in similar models, see e.g., Refs. [63–66].

Once the ansatz (5) for the effective action is specified, the Wetterich equation (2) into a PDE for the effective potential $V_k(\varrho)$. For a concrete result, we also have to choose a regulator which satisfies the conditions we described in the previous section. Here, we use the so-called Litim regulator [52]

$$\begin{aligned} R_k(q,p) &= (2\pi)^d \delta^{(d)}(q+p) p^2 r_k(p), \\ r_k(p) &= \left(\frac{k^2}{p^2} - 1\right)\Theta\left(\frac{k^2}{p^2} - 1\right), \end{aligned} \tag{6}$$

where $r_k(p)$ is the corresponding regulator shape function. A detailed derivation of the flow equation is for example presented in Refs. [8,9]. Here, we simply provide the result,

$$\partial_k V_k(\varrho) = A_d k^{d+1}\left[\frac{N-1}{k^2 + V_k'(\varrho)} + \frac{1}{k^2 + V_k'(\varrho) + 2\varrho V_k''(\varrho)}\right], \tag{7}$$

with

$$A_d = \frac{\Omega_d}{d(2\pi)^d}, \qquad \Omega_d = \frac{2\pi^{d/2}}{\Gamma(d/2)}, \tag{8}$$

where, Ω_d is the volume of the $d-1$ dimensional unit sphere and Γ is the gamma function.

C. FRG flow equation in terms of the field σ and boundary conditions

Up to now the PDE (7) for the effective potential is written in terms of the $O(N)$-invariant ϱ. However, when solving the PDE with a numerical scheme that relies on a discretization in the ϱ-direction, we face the following problem. Usually, such a numerical scheme requires a stencil of points in the vicinity of any given point in the domain where $V_k(\varrho)$ is defined. In particular, this stencil is then also required at the boundary $\varrho = 0$, i.e., we would have to specify $V_k(\varrho)$ for some negative value of ϱ, which does not exist.

A solution is to reformulate the equations above in terms of the field expectation value $\sigma = \sqrt{2\varrho}$, i.e., we consider $V_k(\sigma)$, $\partial_\sigma V_k(\sigma)$, and $\partial_\sigma^2 V_k(\sigma)$ instead of $V_k(\varrho)$, $\partial_\varrho V_k(\varrho)$, and $\partial_\varrho^2 V_k(\varrho)$, respectively. We then rewrite Eq. (7) as follows:

$$\partial_k V_k(\sigma) = A_d k^{d+1}\left[\frac{N-1}{k^2 + \frac{1}{\sigma}\partial_\sigma V_k(\sigma)} + \frac{1}{k^2 + \partial_\sigma^2 V_k(\sigma)}\right]. \tag{9}$$

The boundary condition at $\sigma = 0$ (including points in its vicinity) is now specified exploiting the residual $\mathbb{Z}_2$ symmetry of the potential,

$$V_k(\sigma) = V_k(-\sigma), \tag{10}$$

which translates into a $\mathbb{Z}_2$ antisymmetry for $\partial_\sigma V_k(\sigma)$,

$$\partial_\sigma V_k(\sigma) = -\partial_\sigma V_k(-\sigma), \tag{11}$$

and again a $\mathbb{Z}_2$ symmetry for $\partial_\sigma^2 V_k(\sigma)$,

$$\partial_\sigma^2 V_k(\sigma) = \partial_\sigma^2 V_k(-\sigma). \tag{12}$$

The PDE (9) cannot be solved numerically on an infinite domain $\sigma \in [0, \infty)$. Therefore, we have to choose a sufficiently large value of σ for the upper boundary, say $\sigma_{\max}$, and we also need to specify $V_k(\sigma_{\max})$.

In the UV, at $k \to \infty$, the effective potential $V_k(\sigma)$ is given by the potential term in the bare action S_{bare}, which is usually a polynomial in powers of σ. For a $\mathbb{Z}_2$-symmetric potential, these powers must be even. For an interacting theory, the smallest power of σ in the interaction term must then be at least four. This means that for large σ the right-hand side of the FRG flow equation (9) is at least of order $\sim\sigma^{-2}$. Choosing a sufficiently large $\sigma_{\max}$ ensures that the right-hand side of Eq. (9) can be neglected, which means that the effective potential $V_k(\sigma_{\max})$ does not change under the FRG flow and stays at its UV value. For a more detailed discussion on the boundary conditions and how to implement them we refer to Ref. [31].

D. Advection-diffusion formulation of the FRG flow equation

For the sake of convenience, let us introduce the "RG-time" parameter t via

$$t = -\ln\left(\frac{k}{\Lambda}\right), \qquad \frac{\partial}{\partial t} = -k\frac{\partial}{\partial k}. \tag{13}$$

Note that we choose the opposite sign as in most of the standard FRG literature, because we deem it more natural for a time to flow from $t = 0$ (at $k = \Lambda$) to $t = \infty$ (at $k = 0$).

We will now show that it is possible to cast Eq. (9) into the form of an advection-diffusion equation well-known from hydrodynamics. This is possible because Eq. (9) is independent of the potential itself and thus one can rewrite it in terms of a PDE for

$$u(t, \sigma) = \partial_\sigma V(t, \sigma). \tag{14}$$

Analogously we will denote

$$u'(t, \sigma) = \partial_\sigma u(t, \sigma) = \partial_\sigma^2 V(t, \sigma). \tag{15}$$

Here, we have defined $V(t, \sigma) = V_k(\sigma)$, i.e., we replaced the k-dependence of $V_k(\sigma)$ by an equivalent dependence on the variable t. We also considered $V(t, \sigma)$ as a function of the two continuous variables t and σ. In the interpretation of the FRG flow equation as an advection-diffusion equation, t will retain its role as a time variable for the FRG flow, while σ will assume the role of a spatial variable. The main advantage of considering the FRG flow equation as an advection-diffusion equation is that it allows us to exploit the powerful toolbox of numerical methods that have been developed to solve hydrodynamical equations.

We now introduce the function

$$f(t, u, \sigma) = (N-1)A_d \frac{(\Lambda e^{-t})^{d+2}}{(\Lambda e^{-t})^2 + \frac{1}{\sigma}u(t, \sigma)}, \tag{16}$$

which corresponds to the nonlinear advection flux in the hydrodynamical interpretation, as well as the function

$$g(t, u') = -A_d \frac{(\Lambda e^{-t})^{d+2}}{(\Lambda e^{-t})^2 + u'(t, \sigma)}, \tag{17}$$

which corresponds to a nonlinear diffusion flux. Taking the derivative of Eq. (7) with respect to σ we then obtain the equation for $u(t,\sigma)$ as

$$\partial_t u(t,\sigma) + \partial_\sigma f(t,u,\sigma) = \partial_\sigma g(t,u'), \tag{18}$$

which has exactly the form of a nonlinear advection-diffusion equation for some fluid field u. For more details on the properties of this equation in the FRG framework we refer to Refs. [29–36].

IV. CRITICAL BEHAVIOR

In order to study the critical behavior of the $O(N)$ model, we first have to set an initial condition for the FRG flow in the UV, i.e., at $t = 0$ or $k = \Lambda$. The potential in the UV is chosen to have the well-known ϕ^4 form,

$$V_{k=\Lambda}(\varrho) = \frac{\lambda}{4}(\varrho - \varrho_0|_{t=0})^2, \tag{19}$$

where $\varrho_0|_{t=0}$ is the minimum of the potential at $k = \Lambda$. For $\varrho_0|_{t=0} > 0$, the system is in the broken phase, while for $\varrho_0|_{t=0} = 0$ it is in the symmetric phase.

In particular, in the case where $\varrho_0|_{t=0} > 0$, one component of the N-dimensional scalar field $\vec{\phi}$ develops a nonvanishing expectation value and the $O(N)$-symmetry group is spontaneously broken to $O(N-1)$. According to Goldstone's theorem, this leads to $N-1$ massless modes, the so-called Nambu-Goldstone bosons. The remaining component of the field $\vec{\varphi}$ is the radial σ mode discussed above in Sec. III C, which develops a nonvanishing mass proportional to the minimum $\varrho_0|_{t=0}$ [67]. For example, considering the model at finite temperatures, the $O(N)$ symmetry is restored via a second-order phase transition and all modes become degenerate in mass when the temperature is increased above a critical value.

It seems clear that, due to the nonperturbative nature of the phase transition, a simple perturbative approach fails to describe this phenomenon. On the other hand, the nonperturbative FRG approach allows us to go beyond any finite order in perturbation theory, and thus to correctly treat this kind of problem. Via this approach we will determine several critical exponents in the LPA.

A. Critical scaling

In order to compute the critical exponents we need the generalization of the flow equation (9) to finite temperature. However, we can circumvent this step by exploiting the well-known phenomenon of dimensional reduction [68–71]; in the limit of high temperatures, or more precisely, when the temperature is much larger than the FRG flow parameter, $T \gg k$, the nonzero Matsubara modes with energy $\sim 2\pi n T$, $n \neq 0$, decouple from the evolution, leaving only a three-dimensional effective theory involving the zero Matsubara mode. From a different perspective, if the correlation length, which is the scale associated with the system, dominates over the inverse temperature, then it is not possible to resolve the compactified Euclidean time dimension, leading to a dimensionally reduced effective theory. Thus, we do not need to use a finite-temperature flow equation in order to investigate the critical region of the phase transition. Instead, it is sufficient to employ the $(d = 3)$-dimensional zero-temperature equation (9).

According to universality-class arguments [72–75], there are two relevant parameters that can be tuned in order to bring the system to the critical point. This can be immediately understood considering the ferromagnetic Ising model, which has a discrete $\mathbb{Z}_2 = O(1)$ symmetry, as an example: here the parameters that drive the system towards the phase transition are the temperature and the external magnetic field. Since we are considering the $O(N)$ model without external fields, only one relevant parameter is left in our case: the temperature.

However, since we exploit the dimensional-reduction phenomenon and work in a zero-temperature field theory, the temperature does not explicitly enter the description and we need to identify a relevant variable which assumes its role. Obviously, such a variable decides whether the system ends up in the symmetric or broken phase when $t \to \infty$. This leads us to take the UV minimum $\varrho_0|_{t=0}$ of the potential as the variable replacing the temperature. Indeed, if $\varrho_0|_{t=0}$ is larger than a critical value $\varrho_0^c|_{t=0}$, the system will end up in the broken phase in the IR, i.e., this is equivalent to working at temperatures $T < T_c$. Analogously, if $\varrho_0|_{t=0} < \varrho_0^c|_{t=0}$, the system will end up in the symmetric phase in the IR, which is equivalent to working at temperatures $T > T_c$.

Due to the convexity of the effective potential, see for example Ref. [76], in the broken phase the potential $V_{\mathrm{IR}}(\sigma)$ is flat for $\sigma \leq \sigma_0|_{\mathrm{IR}}$, where $\sigma_0|_{\mathrm{IR}} = \sqrt{2\varrho_0|_{\mathrm{IR}}} > 0$ is the minimum of the potential in the IR, i.e., for $t \to \infty$. On the other hand, in the symmetric phase $\sigma_0|_{\mathrm{IR}} = 0$. This allows us to identify $\sigma_0|_{\mathrm{IR}}$ as the *order parameter* of the phase transition, since $\sigma_0|_{\mathrm{IR}} > 0$ in the broken phase and $\sigma_0|_{\mathrm{IR}} = 0$ in the symmetric one.

This qualitative discussion is confirmed by solving the FRG flow equation, cf. Fig. 1, where we plot the effective potential $V_k(\sigma)$ (right panel) and its derivative $u(t,\sigma)$ (left panel) for different values of $\sigma_0|_{t=0}$ at the FRG time $t = 3$, which is sufficiently far in the IR such that the flow does not change the minimum of the potential and the curvature mass at the minimum by an appreciable amount (for a detailed discussion of the numerical errors, see Sec. V).

One observes that, for small values of $\sigma_0|_{t=0}$ the system ends up in the symmetric phase in the IR ($\sigma_0|_{\mathrm{IR}} = 0$), while for larger values of $\sigma_0|_{t=0}$ the symmetry remains broken in the IR ($\sigma_0|_{\mathrm{IR}} > 0$) and the potential exhibits a plateau. Since we are dealing with a second-order phase transition,

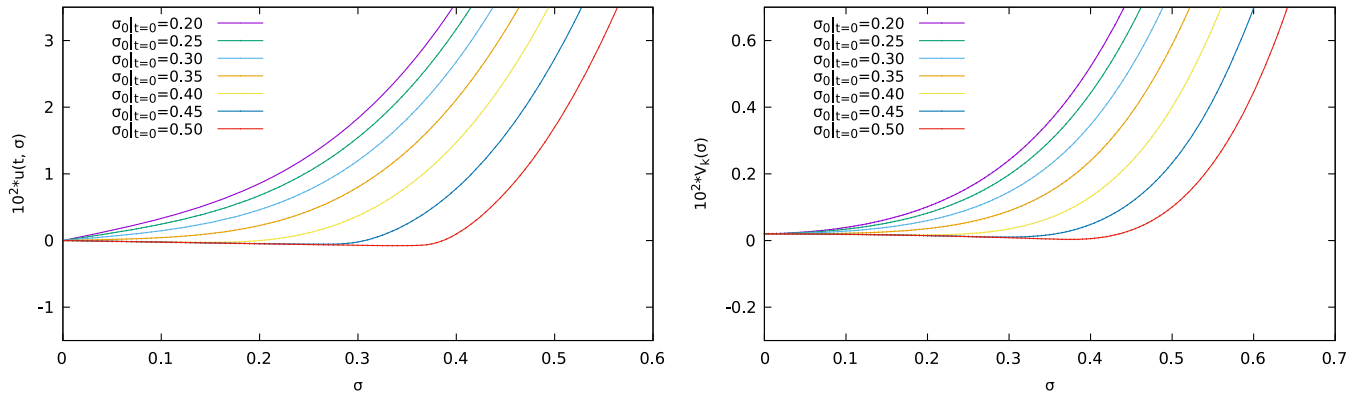

FIG. 1. The effective potential $V_k(\sigma)$ (right panel) and its derivative $u(t,\sigma)$ (left panel) in LPA at RG time $t = 3$, for different values of $\sigma_0|_{t=0} = \sqrt{2\varrho_0|_{t=0}}$ and for $N = 3$. The UV cutoff scale is $\Lambda = 1.0$, the grid size is $[0, \sigma_{\max}] = [0, 2.0]$, while the grid spacing is $\Delta\sigma = 0.005$ (corresponding to 400 grid points).

we expect an IR fixed point of the FRG flow, close to which the theory is scale-invariant. Thus the critical behavior has to be described by a solution of the FRG flow equation which is scale-independent for sufficiently small (large) values of k (t). Since we only have one relevant variable ($\varrho_0|_{t=0}$), we are allowed to set λ, which is an irrelevant variable from the RG perspective, to an arbitrary value. Here, we choose $\lambda = 0.5$. We then tune $\varrho_0|_{t=0}$ in order to find the so-called *scaling solution* or *critical trajectory*, i.e., a solution of the FRG flow equation which becomes t independent for sufficiently large values of t.

In particular, the closer $\varrho_0|_{t=0}$ is to $\varrho_0^c|_{t=0}$, the closer the solution is to the critical trajectory when approaching the IR. This implies that properly rescaled dimensionless quantities will exhibit a constant behavior at sufficiently large t. In particular, the dimensionless minimum

$$\tilde{\varrho}_{0,k} = k^{2-d}\varrho_{0,k} \tag{20}$$

tends to a constant (fixed-point) value as $\varrho_0|_{t=0}$ approaches $\varrho_0^c|_{t=0}$.

This qualitative behavior is quantitatively confirmed by an explicit solution of the FRG flow equation, as shown in Fig. 2, cf. Ref. [25]. Here we plot the evolution of the dimensionless minimum (20) with t for different initial values $\varrho_0|_{t=0}$. One observes that, during the FRG flow, $\tilde{\varrho}_{0,k}$ approaches the critical trajectory, the asymptotic fixed-point value of which is shown by the red horizontal line. However, eventually it deviates upwards (for initial values $\varrho_0|_{t=0} > \varrho_0^c|_{t=0}$) or downwards (for initial values $\varrho_0|_{t=0} < \varrho_0^c|_{t=0}$). This can be easily explained by considering that, in $d = 3$ dimensions:

(i) In the broken phase ($\varrho_0|_{t=0} > \varrho_0^c|_{t=0}$) the minimum $\varrho_{0,k}$ of the potential tends to a constant value $\varrho_0|_{\mathrm{IR}} > 0$ when $k \to 0$, which means that $\tilde{\varrho}_{0,k} = \varrho_{0,k}/k \to +\infty$;

(ii) In the symmetric phase ($\varrho_0|_{t=0} < \varrho_0^c|_{t=0}$) the minimum $\varrho_{0,k}$ of the potential goes to 0 already at a nonzero value of $k > 0$, which means that $\tilde{\varrho}_{0,k} = \varrho_{0,k}/k \to 0$.

The closer the initial value $\varrho_0|_{t=0}$ is to the critical value $\varrho_0^c|_{t=0}$, the larger is the value of t where the deviation from the scaling solution occurs. The critical trajectory, ending in the fixed-point value as $t \to \infty$, can actually not be reached in practice, as it would require infinite numerical precision and infinite spatial resolution in the domain of the PDE.

Of course not only $\tilde{\varrho}_{0,k}$ exhibits a scaling behavior, but all other appropriately rescaled dimensionless quantities first approach and then deviate from the critical trajectory at certain RG times which depend on the initial value $\varrho_0|_{t=0}$. Here, we choose $\tilde{\varrho}_{0,k}$ since the minimum of the potential is the order parameter characterizing the phase transition.

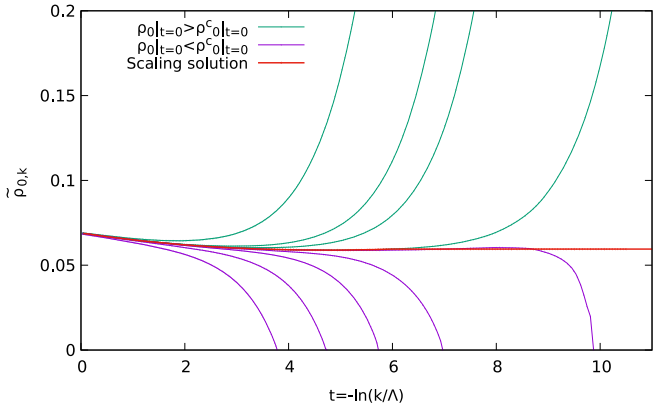

FIG. 2. Scaling of $\tilde{\varrho}_{0,k}$ as a function of RG-time t in the LPA for $N = 3$ and $d = 3$. The calculations are performed for $\Lambda = 1.0$, $\sigma_{\max} = 2.0$, and grid spacing $\Delta\sigma = 0.0005$ (i.e., an order of magnitude smaller than for Fig. 1). The green curves correspond to initial values $\varrho_0|_{t=0} > \varrho_0^c|_{t=0}$, indicating that the system is in the broken phase, while the purple curves correspond to initial values $\varrho_0|_{t=0} < \varrho_0^c|_{t=0}$, i.e., the system is in the symmetric phase. The red horizontal line indicates the fixed-point value of the scaling solution in the IR.

B. Critical exponents

It is a well-known fact [72–75] that some physical quantities derived from the partition function or, equivalently, from the free energy of the system, may diverge when approaching a phase transition, i.e., for $\varrho_0|_{t=0} \to \varrho_0^c|_{t=0}$. In particular they exhibit a *power-law behavior* characterized by so-called *critical exponents*, which depend on the dimension d and the symmetries of the system, and which define the *universality class* of the theory. There exist several critical exponents. However, only two of them are independent, see, e.g., Refs. [77,78]. We consider β and ν as independent and discuss in more detail how to extract them from the FRG flow equation:

(1) *Exponent for the order parameter: β* Close to criticality, the order parameter of the phase transition $\sigma_0|_{\mathrm{IR}}$ is described by the following behavior:

$$\begin{aligned} &\sigma_0|_{\mathrm{IR}} = 0, \qquad \varrho_0|_{t=0} < \varrho_0^c|_{t=0}, \\ &\sigma_0|_{\mathrm{IR}} \sim (\varrho_0|_{t=0} - \varrho_0^c|_{t=0})^{\beta}, \quad \varrho_0|_{t=0} > \varrho_0^c|_{t=0}. \end{aligned} \tag{21}$$

In Fig. 3, we show $\ln(\sigma_0|_{\mathrm{IR}})$ as a function of $\ln(\varrho_0|_{t=0} - \varrho_0^c|_{t=0})$ for $N = 3$ and $d = 3$ in the LPA. The exponent β is then read off from the slope of this function.

One observes that, for small values of $\ln(\varrho_0|_{t=0} - \varrho_0^c|_{t=0})$, $\ln(\sigma_0|_{\mathrm{IR}})$ deviates from the scaling behavior given by the second line of Eq. (21). This deviation is caused by the finite numerical precision with which we can determine $\varrho_0^c|_{t=0}$. The closer the initial $\varrho_0|_{t=0}$ is to the critical value, the more sensitive one is to deviations from the actual critical value caused by the finite numerical precision, and thus one simply does not follow the critical behavior anymore.

Note that, if we work in the finite-temperature theory, $\sigma_0|_{\mathrm{IR}}$ would be a function of temperature and close to criticality would be proportional to $(T_c - T)^{\beta}$. Thus $\varrho_0^c|_{t=0}$ determines the critical temperature in three dimensions.

(2) *Exponent for the correlation length: ν* For large spatio-temporal distances, the correlator exhibits an exponential decay,

$$\begin{aligned} G(x-y) &= \langle \phi(x)\phi(y)\rangle - \langle \phi(x)\rangle\langle \phi(y)\rangle \\ &\sim e^{-|x-y|/\xi} \quad \text{for } |x-y| \gg \xi, \end{aligned} \tag{22}$$

where ξ is the so-called *correlation length*. Close to criticality it behaves as

$$\xi(T) \sim (T - T_c)^{-\nu}, \tag{23}$$

which, in the dimensionally reduced theory, becomes

$$\xi(\varrho_0|_{t=0}) \sim |\varrho_0|_{t=0} - \varrho_0^c|_{t=0}|^{-\nu}. \tag{24}$$

In order to compute ν, we exploit the fact that the correlation length is proportional to the inverse of the renormalized mass m, $\xi \sim m^{-1}$. Note that in the LPA the pole, curvature, and screening masses are identical for zero-temperature calculations [79]. In the symmetric phase, the square of the renormalized mass is given by

$$m^2 = \lim_{t\to\infty} u'(t, \sigma = 0) = \lim_{t\to\infty} \partial_\sigma^2 V(t, \sigma = 0). \tag{25}$$

Thus we compute m^2 and then exploit

$$m^2 \sim |\varrho_0|_{t=0} - \varrho_0^c|_{t=0}|^{2\nu}. \tag{26}$$

In this way we can obtain ν from the slope of $\ln m^2$ as a function of $\ln|\varrho_0|_{t=0} - \varrho_0^c|_{t=0}|$, see Fig. 4. We note that one has to make sure to reach the symmetric

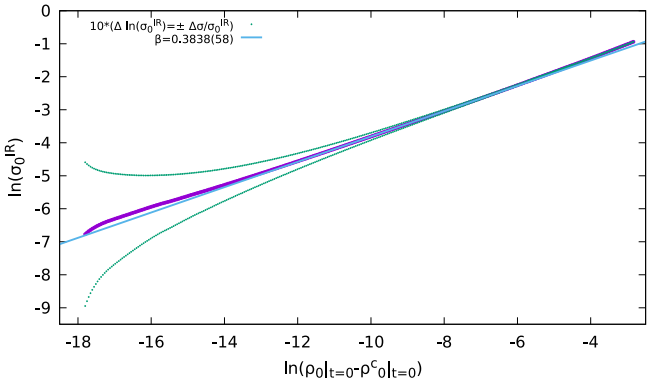

FIG. 3. Double-logarithmic plot of Eq. (21) (violet dots) in the LPA case for $N = 3$ and $d = 3$. The green dots mark the boundaries of the error band. The slope of the blue line gives the estimate for the critical exponent β. Other parameters of the calculation are the same as for Fig. 2.

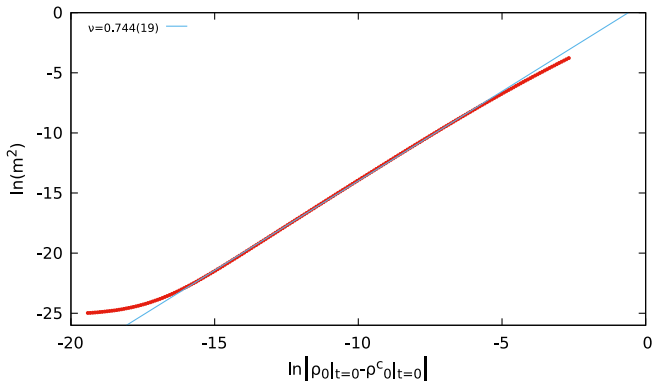

FIG. 4. Double-logarithmic plot of Eq. (26) (red dots) in the LPA case for $N = 3$ and $d = 3$. The slope of the blue line gives twice the value of the critical exponent ν. Other parameters of the calculation are the same as for Fig. 2.

TABLE I. Order parameter exponent β.

N	LPA	RG'	MC	PT	ε-expansion	CB	DE_4
1	0.3486(59)	0.32	0.32643(6)	0.3258(10)	0.32599(32)	0.326419(2)	0.3263(4)
2	0.3659(45)	0.35	0.34864(5)	0.3470(11)	0.3472(6)	0.34872(5)	0.3485(5)
3	0.3838(58)	0.37	0.3689(3)	0.366(2)	0.366(1)	0.3697(12)	0.3691(7)
4	0.4046(34)	0.40	0.3873(4)	0.3834(35)	0.3834(18)	0.3877(47)	0.3874(6)
10	0.4541(45)	0.45			0.4398(7)	0.4523(2)	0.4489(6)

TABLE II. Correlation length exponent ν.

N	LPA	RG'	MC	PT	ε-expansion	CB	DE_4
1	0.634(8)	0.64	0.63002(10)	0.6304(13)	0.6292(5)	0.629971(4)	0.62989(25)
2	0.7057(14)	0.69	0.67169(7)	0.6703(15)	0.6690(10)	0.6718(1)	0.6716(6)
3	0.744(19)	0.74	0.7112(5)	0.7073(35)	0.7059(20)	0.7120(23)	0.7114(9)
4	0.780(20)	0.78	0.7477(8)	0.741(6)	0.7397(35)	0.7472(87)	0.7478(9)
10	0.901(13)	0.91			0.859(1)	0.8842(3)	0.8776(10)

phase before stopping the t-evolution, because only this ensures that $m^2 > 0$ at $\sigma = 0$.

We remark that the deviation of $\ln m^2$ from the scaling solution at small values of $\ln|\varrho_0|_{t=0} - \varrho_0^c|_{t=0}|$ has the same origin as that observed in Fig. 3. On the other hand, the deviation observed for large values of $\ln|\varrho_0|_{t=0} - \varrho_0^c|_{t=0}|$ is due to the fact that one is simply too far away from the critical region, such that the scaling behavior of Eq. (22) does no longer apply.

In Tables I and II we show our results for β and ν, respectively, obtained within the LPA for $d = 3$ and various values of N in comparison to results obtained within similar as well as other frameworks. Results obtained within the same FRG framework but including a nontrivial RG scale-dependent wave-function renormalization [25] are denoted as "RG' ". Results obtained from Monte Carlo (MC) simulations [80,81] are listed under "MC", those from perturbative RG are denoted as "PT" [82], while those from the ε-expansion at order ε^6 are shown under "ε-expansion" [83]. Results from conformal bootstrap (CB) are denoted as "CB" [84–86], and finally those from a derivative expansion up to fourth order as "DE_4" [24]. We observe that the results obtained in this work are overall in good agreement with the ones obtained with other approaches. As compared to the results of RG', which is from a technical perspective closest to our approach, we improve the precision by one order of magnitude and in addition provide an error estimate, see Sec. V for details. Although RG' includes a nontrivial wave-function renormalization, while our approach does not, our results for the values of the critical exponents are not significantly worse than RG'. Furthermore, we have checked that the values obtained for finite N tend to converge to the ones in the large-N limit, shown in Table III, since in that case the LPA becomes exact [47].

V. NUMERICAL PRECISION AND ERROR ESTIMATES

In order to provide some insight into the capabilities and limitations of our method, in this section we discuss the numerical precision of our results and give error estimates. There is of course a systematic error due to the use of the LPA [21,24], which can be estimated by improving the truncation beyond LPA [24,25,27,28]. This, however, is beyond the scope of the current paper. Moreover, there are also fit errors which result from the way the critical exponents are determined. One of them is general in the sense that it is inherent to the extraction of both β and ν, but there are also some which are specific for the calculation of either ν or β.

A. General fit error

As discussed in Sec. IV, a linear fit to the data is performed, the slope of which gives the critical exponents. This procedure inevitably leads to some error due to the fact that, as mentioned in Sec. IV, some points do not follow the critical scaling and thus deviate from the linear fit. Therefore, we need a criterion which enables us to select which points we should take into account for the fit. This is an important issue, since, as can be seen from Figs. 6 and 7, the value of a particular critical exponent and the relative fit error may change a lot if only a single data point is added to (or subtracted from) the fit. Since our goal is to extract the critical exponents from the scaling region, where we expect

TABLE III. Critical exponents in the large-N case.

	β	ν	η	δ	α	γ
Large N	0.5	1.0	0	5	−1.0	2.0

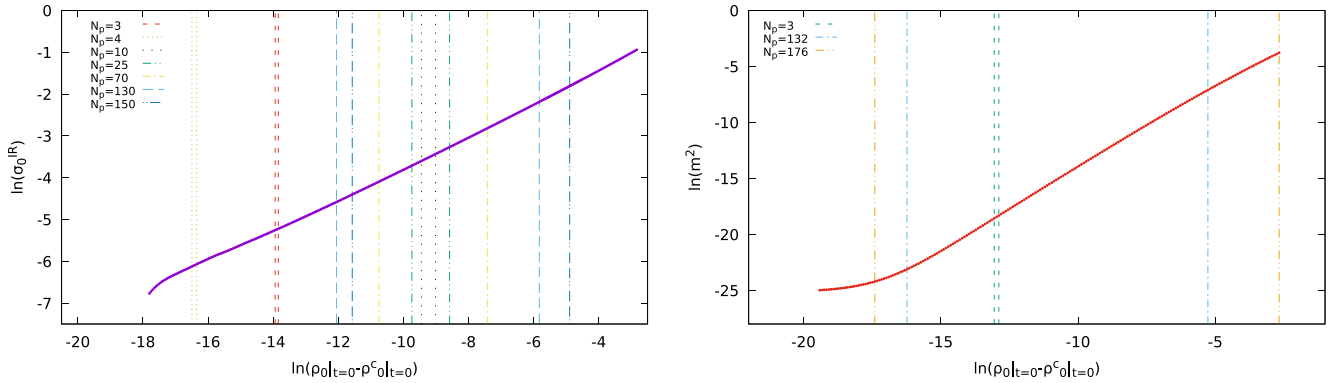

FIG. 5. Different fitting regions corresponding to different numbers of most aligned consecutive points, for the extraction of the critical exponents β (left panel) and ν (right panel). Here, $N = 3$ and $d = 3$. Other parameters of the calculation are the same as for Fig. 2.

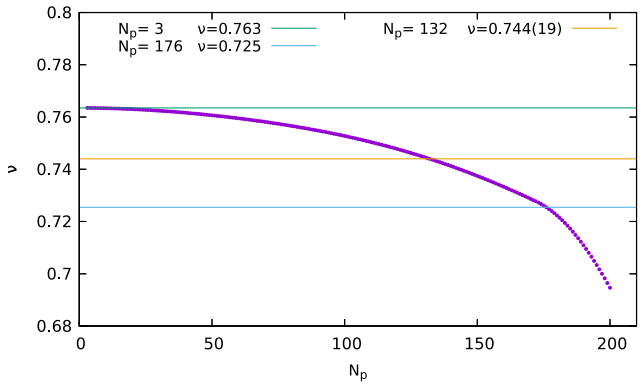

FIG. 6. Critical exponent ν as a function of the number of the most aligned points N_p taken into consideration in the fit, for the case $N = 3$ and $d = 3$. Other parameters of the calculation are the same as for Fig. 2.

a linear behaviour of the observables (the logarithm of the IR minimum and the logarithm of the curvature mass) as a function of $\ln|\varrho_0|_{t=0} - \varrho_0^c|_{t=0}|$, it seems reasonable to use those consecutive points for the fit which exhibit the highest degree of collinearity. As a criterion for collinearity, we choose the Pearson correlation coefficient. However, the range of points which is taken into consideration still has a significant impact on the value of the critical exponents. This can be clearly seen from Figs. 6 and 7, where the critical exponents are shown as a function of the number of consecutive most aligned points. This is due to the fact that, as shown in Fig. 5, either the region where the consecutive most aligned points are contained moves while modifying the number of points, or it includes points in the fit which are increasingly further away from a straight fitting line. Thus, a criterion is still needed according to which one should select the number of consecutive collinear points.

It is worth noting that the behavior seen in Figs. 6 and 7 is not affected by varying the point density (number of points per unit interval of the fitting region), indicating that the values of the critical exponents depend on the size of the fitting region rather than on the number of points contained in it. Ideally, if all points belong to the scaling region, all of them would exhibit perfect collinearity and thus the critical exponents would become completely independent of the fitting region.

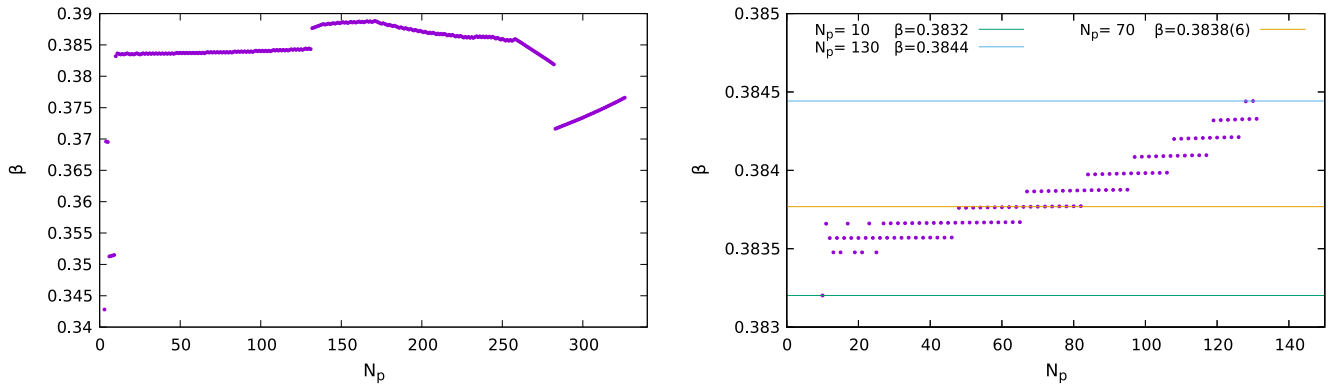

FIG. 7. Critical exponent β as a function of the number of the most aligned points N_p taken into consideration in the fit (left panel). The right panel is zooming in on the region where the value of the critical exponent is least dependent on N_p. In both plots $N = 3$ and $d = 3$. Other parameters of the calculation are the same as for Fig. 2.

Our criterion is thus to identify the scaling region by searching for the range on the abscissa in Figs. 6 and 7 where the critical exponent is least dependent on the number of consecutive collinear points and thus on the fitting region. Once this range is identified, we assume that the actual value of the critical exponent lies somewhere between the highest and the lowest value of the critical exponent in that range. This gives a contribution to the total error on the critical exponent which is half the difference of the highest and the lowest value in that range. Finding such a range of consecutive collinear points is straightforward in the case of β: if the number of points in the range considered is too small, the range moves a lot along the abscissa when it is extended. Therefore, we discard the leftmost points in Fig. 7 (left panel). From a certain size onward the range does not move anymore, but merely grows within the critical region. However, if the range is too large, also points from outside the critical region are included, which is clearly seen by the jump in Fig. 7 (left panel) at $N_p \simeq 130$. Hence, this clearly restricts the size of the critical region.

On the other hand, in the case of ν, if the fitting region is too large, the exponent starts to change more rapidly, indicating that the corresponding fitting region includes points which do not follow a straight line in Fig. 4. Thus, we restricted the fit to a maximum value of $N_p \simeq 180$. However, from Fig. 6 it is clearly visible that it is much harder, if not almost impossible, to identify a critical region, because ν strongly depends on the fitting interval.

We conclude this subsection by first noticing that the error originating from the choice of the fitting region is much larger than the error of the fit itself, i.e., the one extracted from the maximum deviation of the points in the fitting region from a straight line. Indeed, this error is at least one order of magnitude smaller than the error from the choice of the fitting region. Second, as we discuss next, the error from choosing the correct fitting region is also much larger than the numerical error coming from the KT scheme and the determination of the curvature mass, which is required for extracting ν. For β, however, the discretization error, which results in an uncertainty on the position of the minimum, is again comparable to the error arising from the determination of the size of the critical region.

B. Error on m^2

In this subsection we analyze the impact of the discretization in field space, i.e., of the grid spacing $\Delta\sigma$, on the value of the renormalized mass m^2 and on the corresponding error. In Fig. 8, we show the curvature mass squared m^2 (left panel) and its relative deviation (right panel)

$$\Delta m^2_{\mathrm{rel}}(\Delta\sigma) = 1 - \frac{m^2(\Delta\sigma)}{m^2(\Delta\sigma_{\mathrm{min}})} \tag{27}$$

from the value $m^2(\Delta\sigma_{\mathrm{min}})$ calculated for the smallest cell size $\Delta\sigma_{\mathrm{min}}$ (which in our case is 10^{-4}) as a function of $\Delta\sigma$. Note that each point in these figures is the result of an FRG flow evolution, obtained for $\sigma_0|_{t=0} = 0.3$ in the symmetric phase ($\sigma_0^{\mathrm{IR}} = 0$) at final time $t_{\mathrm{IR}} = 25$ ($k_{\mathrm{IR}} \sim 10^{-11}$). The aim is to identify the value of m^2 from a plateau region, i.e., when its value does not change anymore upon changing the value of $\Delta\sigma$. From Fig. 8 we observe that this happens for values of $\Delta\sigma \lesssim 10^{-2.5}$. Thus, in order to get a reasonable compromise between computational resources and needed precision, we use $\Delta\sigma = 0.0005$ (corresponding to the fourth point from the left in Fig. 8 (left panel)). As one observes from the right panel of Fig. 8, this choice leads to a relative error in the determination of m^2 of the order of $\sim e^{-7} \simeq 10^{-3}$.

As anticipated, the right panel provides an estimate of the order of magnitude of the relative errors, which is especially useful for those points which belong to the plateau in the left panel. The fact that these relative differences scale as $\Delta\sigma^{\alpha}$, with $\alpha > 2$, is a direct consequence of the numerical scheme used, the KT scheme, which has second-order precision in the spatial resolution. This means that it is possible to significantly reduce the error in the

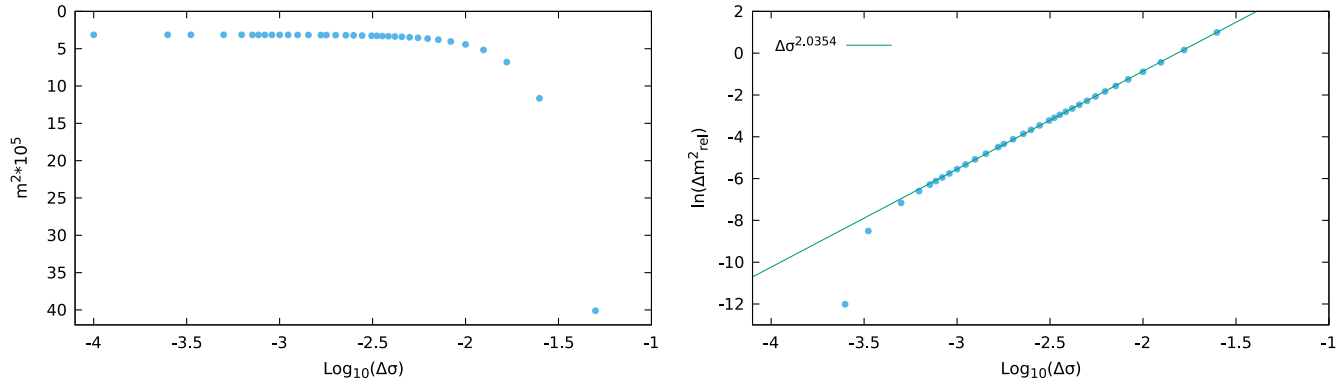

FIG. 8. Curvature mass squared in the IR, m^2 (left panel), and relative deviation of m^2 from the value calculated for the smallest cell size (right panel) as functions of the cell size $\Delta\sigma$. Here, $N = 3$, $d = 3$, $\Lambda = 1.0$, and $\sigma_{\mathrm{max}} = 2.0$.

determination of m^2 by choosing a sufficiently small $\Delta\sigma$. We should also mention that there is no additional error from using a finite-difference stencil in Eq. (25) to extract the curvature mass at $\sigma = 0$, for details see Refs. [31,34].

One final remark is related to the extrapolation of the value of m^2 in the IR. As final value of t in the IR we have chosen $t = 25$, since at this point the FRG flow is effectively frozen in, i.e., no quantity changes anymore with RG time. We convinced ourselves that this is true by computing m^2 for $t = 50$ and $t = 100$. The values of m^2 at these times were the same as at $t = 25$ up to machine precision. Thus, in the symmetric phase it is possible to reach arbitrarily small momentum scales to obtain IR quantities.

C. Error on σ_0^{IR}

Several aspects have to be taken into account regarding the determination of the value of σ_0^{IR}. First of all, in the broken phase, $u(t,\sigma)$ is negative for $\sigma < \sigma_0$ and approaches zero from below as $t \to \infty$. As a consequence, the denominator in Eq. (16) becomes very small when approaching the IR, which leads to a stiff problem when solving the FRG flow equation numerically, i.e., the time step Δt has to become increasingly smaller when $t \to \infty$ in order to avoid numerical instabilities. In practice, this prevents us to go arbitrarily far into the IR within our setup. For recent advances on this issue, we refer to Ref. [87]. This problem is solved by determining the position of the minimum σ_0^{IR} via extrapolation. Here, we decided to perform an exponential extrapolation of σ_0 as a function of k via a linear extrapolation of the values of $\ln\sigma_0$

$$\ln\sigma_0 = ak + b, \Leftrightarrow \sigma_0 = e^b e^{ak}, \tag{28}$$

as can be seen from Fig. 9. This functional form of the extrapolation is motivated by the behavior of σ_0 in the large-N limit, where such an exponential scaling is exact, as can be shown by solving the FRG flow equation analytically via the method of characteristics (see Refs. [29,88]). This extrapolation is the reason for the small oscillations of $\ln\sigma_0^{\mathrm{IR}}$ observed in Fig. 3.

Even if the extrapolation procedure were to give the correct value, the uncertainty on σ_0^{IR} is still limited from below by the grid spacing $\Delta\sigma$. Assuming that the correct value lies within a cell, one can still determine whether σ_0 lies to the left or the right of the cell center, such that the uncertainty is $\Delta\sigma_0^{\mathrm{IR}} \lesssim \Delta\sigma/2$.

Indeed, it can be seen from Fig. 10 that, starting with the same fixed σ_0^{UV}, the position of the minimum is independent of the cell size $\Delta\sigma$ for larger momentum scales and becomes dependent on $\Delta\sigma$ as k decreases (the shifts of the curves in the right panel, which are performed to increase the visibility of the $\Delta\sigma$ bands, are smaller than the actual differences between the curves). However, we observe that, for any given $\Delta\sigma$, for small k the fluctuations of σ_0 as a function of k stay within a band given by $\pm\Delta\sigma/2$, confirming the aforementioned assumption for the error on σ_0^{IR}. In addition, these fluctuations seem to decrease as $\Delta\sigma$ is reduced.

Thus, assuming $\Delta\sigma/2$ as the error on every value of σ_0^{IR}, each point in Fig. 3 has an error given by

$$\delta\ln\sigma_0^{\mathrm{IR}} = \frac{\delta\sigma_0^{\mathrm{IR}}}{\sigma_0^{\mathrm{IR}}} = \frac{\Delta\sigma}{2\sigma_0^{\mathrm{IR}}}. \tag{29}$$

Note that this error depends on σ_0^{IR} itself. We then consider the value of β extracted from the line which passes through the points $((\varrho_0|_{t=0} - \varrho_0^c|_{t=0})^{\mathrm{left}}, \ln\sigma_0^{\mathrm{IR,left}} - \delta\ln\sigma_0^{\mathrm{IR,left}})$ and $((\varrho_0|_{t=0} - \varrho_0^c|_{t=0})^{\mathrm{right}}, \ln\sigma_0^{\mathrm{IR,right}} + \delta\ln\sigma_0^{\mathrm{IR,right}})$, where $\delta\ln\sigma_0^{\mathrm{IR,left}}$ and $\delta\ln\sigma_0^{\mathrm{IR,right}}$ are the errors of the leftmost and rightmost points of the selected fit interval. The difference of this value of β and the one extracted from

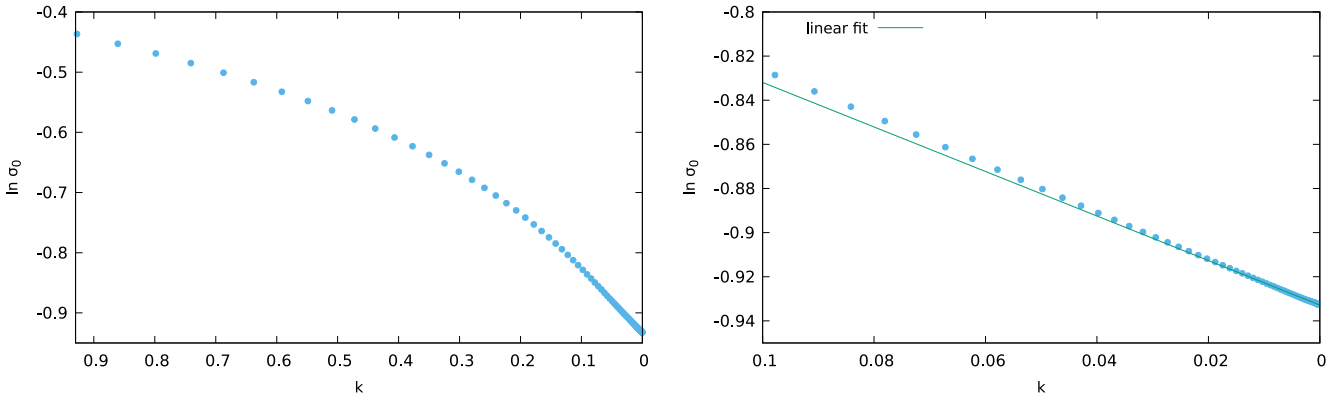

FIG. 9. Logarithm of the minimum σ_0 of the effective potential as a function of the momentum scale k, for $N = 3$ and $d = 3$. The right panel shows the range $0.1 \geq k \geq 0$ from the left panel in higher resolution, with the corresponding linear extrapolation to determine the minimum σ_0^{IR} at $k = 0$. Other parameters of the calculation are the same as for Fig. 2.

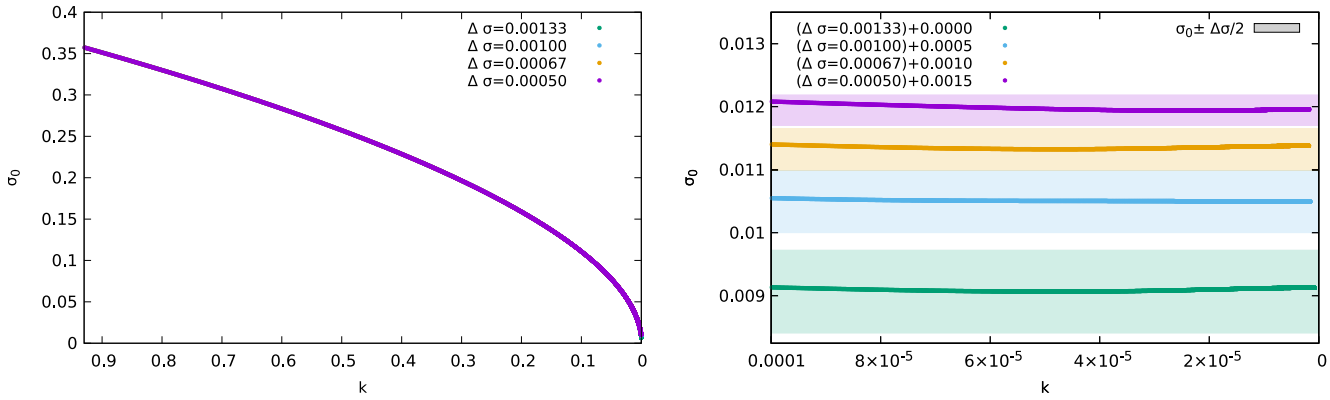

FIG. 10. Position of the minimum of the effective potential σ_0 as a function of the momentum scale k for different values of the cell size $\Delta\sigma$, for $N = 3$ and $d = 3$. The right panel shows the range $0.0001 \geq k \geq 0$ from the left panel in higher resolution, where the fluctuations in the value of σ_0 can be seen. Each band around a line has a width $\Delta\sigma$. In order to avoid overlapping bands, we have performed a global shift of σ_0 for the cases $\Delta\sigma = 0.001$, 0.00067, and 0.0005 by 0.0005, 0.001, and 0.0015, respectively. Other parameters of the calculation are the same as for Fig. 2.

the slope of the straight line in Fig. 3 gives our estimate for $\delta\beta$, which then reads

$$\delta\beta = \frac{\delta \ln \sigma_0^{\mathrm{IR,left}} + \delta \ln \sigma_0^{\mathrm{IR,right}}}{\Delta\varrho_{\mathrm{fit}}}, \tag{30}$$

where $\Delta\varrho_{\mathrm{fit}}$ is the range in $\ln(\varrho_0|_{t=0} - \varrho_0^c|_{t=0})$ where the linear fit is performed.

Using typical values encountered during the calculations, i.e., $\Delta\varrho_{\mathrm{fit}} \simeq 3.5$, $\Delta\sigma = 0.0005$ one finds

$$\delta\beta \simeq 0.006. \tag{31}$$

We will assume this as error on the critical exponent β. It is worth noticing that this contribution is significantly larger than the one coming from the fit error, i.e., the one extracted from the maximum deviation of the points from the straight-line fit, which is usually of order

$$\delta\beta_{\mathrm{fit}} \sim 0.0002. \tag{32}$$

If one wants to have an upper and lower bound for the error, one can use the minimum and the maximum value for σ_0^{IR} in the fit region in Eq. (30). One gets

$$\delta\beta_{>} = 0.024 \quad \delta\beta_{<} = 0.007. \tag{33}$$

Thus, our estimate of the error seems a good compromise between the highest and the lowest possible errors.

VI. CONCLUSION AND OUTLOOK

In this work we have applied the FRG approach to reanalyze the critical exponents of the $O(N)$ model. We exploited the recent realization that the FRG flow equation for the effective potential can be put into the form of an advection-diffusion equation [29], allowing us to employ widely used and well-tested hydrodynamic algorithms to solve it. We demonstrated the feasibility of this approach for the computation of the $O(N)$ critical exponents by solving the FRG flow equation in the LPA. As hydrodynamic algorithm, we used a finite-volume method, the so-called KT scheme [44]. The critical exponents of the $O(N)$ model have been studied previously within the FRG approach in LPA and our discussion closely follows Ref. [25]. However, here, we demonstrated that the novel hydrodynamic approach to solve the FRG flow equations allows a better control of statistical errors. With this method, we have determined these errors much more precisely than in previous work and found them to be of order 10^{-2} to 10^{-3}. They are thus comparable to the errors of other well-established methods like lattice calculations, perturbation theory, the ε-expansion, or CB.

The range of applicability for the novel hydrodynamic method to solve FRG flow equations is very wide. Studies in the framework of the $O(N)$ model were already carried out including higher-order terms in gradients, such as wave-function renormalization factors [24,25,27,28]. Combining these high-precision studies with our developments is certainly a worthwhile future project. Furthermore, it is possible to study the system at finite temperature, without exploiting dimensional reduction. In particular, we expect that the nonzero Matsubara modes do not influence the exponents related to the singular part of free energy (the effective action), that is α, γ, η, ν, while in principle they could give contributions to the order parameter, thus modifying β, and to the critical isotherm, changing the value of δ.

Another possibility is to extend the model to include fermions. From a mathematical point of view, the FRG flow

equations is still an advection-diffusion equation, but now with a source term [30,34,89], which can also be solved using the approach described above.

ACKNOWLEDGMENTS

The authors gratefully acknowledge helpful discussions with L. Kiefer, L. Pannullo, O. Philipsen, M. J. Steil, and N. Wink. This work is supported by the Deutsche Forschungsgemeinschaft (DFG, German Research Foundation) through the Collaborative Research Center CRC-TR 211 "Strong-interaction matter under extreme conditions"—Project No. 315477589—TRR 211 and by the State of Hesse within the Research Cluster ELEMENTS (Project ID No. 500/10.006).

[1] A. Durrant, *Quantum Physics of Matter*, 1st ed. (CRC Press, Location Boca Raton, 2000), 10.1201/9780367807344.
[2] J. Bardeen, L. N. Cooper, and J. R. Schrieffer, Microscopic theory of superconductivity, Phys. Rev. **106**, 162 (1957).
[3] B.-J. Schaefer, M. Wagner, and J. Wambach, Thermodynamics of $(2+1)$-flavor QCD: Confronting models with lattice studies, Phys. Rev. D **81**, 074013 (2010).
[4] T. Yokota, T. Kunihiro, and K. Morita, Functional renormalization group analysis of the soft mode at the QCD critical point, Prog. Theor. Exp. Phys. **2016**, 073D01 (2016).
[5] M. Reuter, Nonperturbative evolution equation for quantum gravity, Phys. Rev. D **57**, 971 (1998).
[6] R. Percacci and G. P. Vacca, Search of scaling solutions in scalar-tensor gravity, Eur. Phys. J. C **75**, 188 (2015).
[7] J. M. Pawlowski, Aspects of the functional renormalisation group, Ann. Phys. (Amsterdam) **322**, 2831 (2007).
[8] H. Gies, Introduction to the functional RG and applications to gauge theories, Lect. Notes Phys. **852**, 287 (2012).
[9] P. Kopietz, L. Bartosch, and F. Schütz, *Introduction to the Functional Renormalization Group* (Springer, Berlin, Heidelberg, 2010), Vol. 798.
[10] N. Dupuis, L. Canet, A. Eichhorn, W. Metzner, J. M. Pawlowski, M. Tissier, and N. Wschebor, The nonperturbative functional renormalization group and its applications, Phys. Rep. **910**, 1 (2021).
[11] J. Berges, N. Tetradis, and C. Wetterich, Nonperturbative renormalization flow in quantum field theory and statistical physics, Phys. Rep. **363**, 223 (2002).
[12] K. G. Wilson, Renormalization group and critical phenomena. 2. Phase space cell analysis of critical behavior, Phys. Rev. B **4**, 3184 (1971).
[13] K. G. Wilson, Renormalization group and critical phenomena. 1. Renormalization group and the Kadanoff scaling picture, Phys. Rev. B **4**, 3174 (1971).
[14] K. G. Wilson and J. Kogut, The renormalization group and the ϵ expansion, Phys. Rep. **12**, 75 (1974).
[15] K. G. Wilson, The renormalization group: Critical phenomena and the Kondo problem, Rev. Mod. Phys. **47**, 773 (1975).
[16] K. G. Wilson, Problems in physics with many scales of length, Sci. Am. **241**, 140 (1979).
[17] J. Polchinski, Renormalization and effective Lagrangians, Nucl. Phys. **B231**, 269 (1984).
[18] A. Hasenfratz and P. Hasenfratz, Renormalization group study of scalar field theories, Nucl. Phys. **B270**, 687 (1986).
[19] J. Braun, H. Gies, and D. D. Scherer, Asymptotic safety: A simple example, Phys. Rev. D **83**, 085012 (2011).
[20] L. Janssen and H. Gies, Critical behavior of the $(2+1)$-dimensional Thirring model, Phys. Rev. D **86**, 105007 (2012).
[21] D. F. Litim, Critical exponents from optimized renormalization group flows, Nucl. Phys. **B631**, 128 (2002).
[22] J. Borchardt and B. Knorr, Global solutions of functional fixed point equations via pseudospectral methods, Phys. Rev. D **91**, 105011 (2015); **93**, 089904(E) (2016).
[23] J. Borchardt and A. Eichhorn, Universal behavior of coupled order parameters below three dimensions, Phys. Rev. E **94**, 042105 (2016).
[24] G. De Polsi, I. Balog, M. Tissier, and N. Wschebor, Precision calculation of critical exponents in the $O(N)$ universality classes with the nonperturbative renormalization group, Phys. Rev. E **101**, 042113 (2020).
[25] O. Bohr, B. J. Schaefer, and J. Wambach, Renormalization group flow equations and the phase transition in O(N) models, Int. J. Mod. Phys. A **16**, 3823 (2001).
[26] A. Chlebicki and P. Jakubczyk, Analyticity of critical exponents of the $O(N)$ models from nonperturbative renormalization, SciPost Phys. **10**, 134 (2021).
[27] I. Balog, H. Chaté, B. Delamotte, M. Marohnic, and N. Wschebor, Convergence of nonperturbative approximations to the renormalization group, Phys. Rev. Lett. **123**, 240604 (2019).
[28] G. De Polsi, G. Hernández-Chifflet, and N. Wschebor, Precision calculation of universal amplitude ratios in O(N) universality classes: Derivative expansion results at order O(∂4), Phys. Rev. E **104**, 064101 (2021).
[29] E. Grossi and N. Wink, Resolving phase transitions with discontinuous Galerkin methods, arXiv:1903.09503.
[30] E. Grossi, F. J. Ihssen, J. M. Pawlowski, and N. Wink, Shocks and quark-meson scatterings at large density, Phys. Rev. D **104**, 016028 (2021).
[31] A. Koenigstein, M. J. Steil, N. Wink, E. Grossi, J. Braun, M. Buballa, and D. H. Rischke, Numerical fluid dynamics for FRG flow equations: Zero-dimensional QFTs as numerical test cases. I. The O(N) model, Phys. Rev. D **106**, 065012 (2022).
[32] A. Koenigstein, M. J. Steil, N. Wink, E. Grossi, and J. Braun, Numerical fluid dynamics for FRG flow equations:

Zero-dimensional QFTs as numerical test cases. II. Entropy production and irreversibility of RG flows, Phys. Rev. D **106**, 065013 (2022).
[33] M. J. Steil and A. Koenigstein, Numerical fluid dynamics for FRG flow equations: Zero-dimensional QFTs as numerical test cases. III. Shock and rarefaction waves in RG flows reveal limitations of the N → ∞ limit in O(N)-type models, Phys. Rev. D **106**, 065014 (2022).
[34] J. Stoll, N. Zorbach, A. Koenigstein, M. J. Steil, and S. Rechenberger, Bosonic fluctuations in the $(1+1)$-dimensional Gross-Neveu(-Yukawa) model at varying μ and T and finite N, arXiv:2108.10616.
[35] F. Ihssen and J. M. Pawlowski, Functional flows for complex effective actions, SciPost Phys. **15**, 074 (2023).
[36] F. Ihssen, J. M. Pawlowski, F. R. Sattler, and N. Wink, Local discontinuous galerkin for the functional renormalisation group, arXiv:2207.12266.
[37] A. B. Zamolodchikov, Irreversibility of the flux of the renormalization group in a 2D field theory, JETP Lett. **43**, 730 (1986).
[38] G. Zumbach, The Renormalization group in the local potential approximation and its applications to the $O(N)$ model, Nucl. Phys. **B413**, 754 (1994).
[39] N. Tetradis and D. F. Litim, Analytical solutions of exact renormalization group equations, Nucl. Phys. **B464**, 492 (1996).
[40] D. Litim and N. Tetradis, Approximate solutions of exact renormalization group equations, arXiv:hep-th/9501042.
[41] O. J. Rosten, Fundamentals of the exact renormalization group, Phys. Rep. **511**, 177 (2012).
[42] K.-I. Aoki, S.-I. Kumamoto, and D. Sato, Weak solution of the non-perturbative renormalization group equation to describe dynamical chiral symmetry breaking, Prog. Theor. Exp. Phys. **2014**, 043B05 (2014).
[43] K.-I. Aoki, S.-I. Kumamoto, and M. Yamada, Phase structure of NJL model with weak renormalization group, Nucl. Phys. **B931**, 105 (2018).
[44] A. Kurganov and E. Tadmor, New high-resolution central schemes for nonlinear conservation laws and convection–diffusion equations, J. Comput. Phys. **160**, 241 (2000).
[45] C. Wetterich, Exact evolution equation for the effective potential, Phys. Lett. B **301**, 90 (1993).
[46] U. Ellwanger, Flow equations for N point functions and bound states, Z. Phys. C **62**, 503 (1994).
[47] T. R. Morris, On truncations of the exact renormalization group, Phys. Lett. B **334**, 355 (1994).
[48] M. Reuter and C. Wetterich, Effective average action for gauge theories and exact evolution equations, Nucl. Phys. **B417**, 181 (1994).
[49] J. Braun, M. Leonhardt, and J. M. Pawlowski, Renormalization group consistency and low-energy effective theories, SciPost Phys. **6**, 056 (2019).
[50] C. Wetterich, Average action and the renormalization group equations, Nucl. Phys. **B352**, 529 (1991).
[51] T. R. Morris, The exact renormalization group and approximate solutions, Int. J. Mod. Phys. A **09**, 2411 (1994).
[52] D. F. Litim, Optimized renormalization group flows, Phys. Rev. D **64**, 105007 (2001).
[53] J. M. Pawlowski, M. M. Scherer, R. Schmidt, and S. J. Wetzel, Physics and the choice of regulators in functional renormalisation group flows, Ann. Phys. (Amsterdam) **384**, 165 (2017).
[54] J. Braun, T. Dörnfeld, B. Schallmo, and S. Töpfel, Renormalization group studies of dense relativistic systems, Phys. Rev. D **104**, 096002 (2021).
[55] J. Braun *et al.*, Renormalised spectral flows, SciPost Phys. Core **6**, 061 (2023).
[56] B. Bergerhoff and C. Wetterich, Effective quark interactions and QCD propagators, Phys. Rev. D **57**, 1591 (1998).
[57] J. A. Adams, J. Berges, S. Bornholdt, F. Freire, N. Tetradis, and C. Wetterich, Solving nonperturbative flow equations, Mod. Phys. Lett. A **10**, 2367 (1995).
[58] H. Meyer-Ortmanns, Phase transitions in quantum chromodynamics, Rev. Mod. Phys. **68**, 473 (1996).
[59] H. Kleinert, *Gauge Fields in Condensed Matter*, 1st ed. (World Scientific, Singapore, 1989), 10.1142/0356.
[60] L. Hostetler, J. Zhang, R. Sakai, J. Unmuth-Yockey, A. Bazavov, and Y. Meurice, Clock model interpolation and symmetry breaking in O(2) models, Proc. Sci. LATTICE2021 (**2022**) 353 [arXiv:2110.05527].
[61] B. Simon and R. B. Griffiths, The $(\phi^4)_2$ field theory as a classical Ising model, Commun. Math. Phys. **33**, 145 (1973).
[62] M. D'Attanasio and T. R. Morris, Large N and the renormalization group, Phys. Lett. B **409**, 363 (1997).
[63] L. Canet, B. Delamotte, D. Mouhanna, and J. Vidal, Optimization of the derivative expansion in the nonperturbative renormalization group, Phys. Rev. D **67**, 065004 (2003).
[64] J. Eser, F. Divotgey, M. Mitter, and D. H. Rischke, Low-energy limit of the $O(4)$ quark-meson model from the functional renormalization group approach, Phys. Rev. D **98**, 014024 (2018).
[65] F. Divotgey, J. Eser, and M. Mitter, Dynamical generation of low-energy couplings from quark-meson fluctuations, Phys. Rev. D **99**, 054023 (2019).
[66] N. Cichutek, F. Divotgey, and J. Eser, Fluctuation-induced higher-derivative couplings and infrared dynamics of the Quark-Meson-Diquark Model, Phys. Rev. D **102**, 034030 (2020).
[67] S. R. Coleman, R. Jackiw, and H. D. Politzer, Spontaneous symmetry breaking in the O(N) model for large N*, Phys. Rev. D **10**, 2491 (1974).
[68] A. Kocic and J. B. Kogut, Phase transitions at finite temperature and dimensional reduction for fermions and bosons, Nucl. Phys. **B455**, 229 (1995).
[69] E. Cavalcanti, J. A. Lourenço, C. A. Linhares, and A. P. C. Malbouisson, Dimensional reduction of a finite-size scalar field model at finite temperature, Phys. Rev. D **99**, 025007 (2019).
[70] D. U. Jungnickel and C. Wetterich, Flow equations for phase transitions in statistical physics and QCD, in *Proceedings of the Workshop on the Exact Renormalization Group* (1998), pp. 41–113, arXiv:hep-ph/9902316.
[71] A. K. Rajantie, Feynman diagrams to three loops in three-dimensional field theory, Nucl. Phys. **B480**, 729 (1996); **B513**, 761(E) (1998).
[72] S. keng Ma, *Modern Theory of Critical Phenomena*, 1st ed. (Imprint Routledge, New York, 2001), 10.4324/9780429498886.

[73] N. Goldenfeld, *Lectures on Phase Transitions and the Renormalization Group* (CRC Press, Boca Raton, 2018).
[74] J. Cardy, *Scaling and Renormalization in Statistical Physics*, Cambridge Lecture Notes in Physics (Cambridge University Press, Cambridge, England, 1996), 10.1017/CBO9781316036440.
[75] G. Mussardo, *Statistical Field Theory: An Introduction to Exactly Solved Models in Statistical Physics* (Oxford University Press, New York, NY, 2010).
[76] M. Peláez and N. Wschebor, Ordered phase of the $O(N)$ model within the nonperturbative renormalization group, Phys. Rev. E **94**, 042136 (2016).
[77] M. E. Peskin and D. V. Schroeder, *An Introduction to Quantum Field Theory* (Addison-Wesley, Reading, USA, 1995).
[78] J. Zinn-Justin, Quantum field theory and critical phenomena, Int. Ser. Monogr. Phys. **113**, 1 (2002).
[79] A. J. Helmboldt, J. M. Pawlowski, and N. Strodthoff, Towards quantitative precision in the chiral crossover: Masses and fluctuation scales, Phys. Rev. D **91**, 054010 (2015).
[80] M. Hasenbusch, Finite size scaling study of lattice models in the three-dimensional Ising universality class, Phys. Rev. B **82**, 174433 (2010).
[81] M. Campostrini, M. Hasenbusch, A. Pelissetto, P. Rossi, and E. Vicari, Critical exponents and equation of state of the three-dimensional Heisenberg universality class, Phys. Rev. B **65**, 144520 (2002).
[82] R. Guida and J. Zinn-Justin, Critical exponents of the N vector model, J. Phys. A **31**, 8103 (1998).
[83] M. V. Kompaniets and E. Panzer, Minimally subtracted six loop renormalization of $O(n)$-symmetric ϕ^4 theory and critical exponents, Phys. Rev. D **96**, 036016 (2017).
[84] H. Shimada and S. Hikami, Fractal dimensions of self-avoiding walks and Ising high-temperature graphs in 3D conformal bootstrap, J. Stat. Phys. **165**, 1006 (2016).
[85] S. M. Chester, W. Landry, J. Liu, D. Poland, D. Simmons-Duffin, N. Su, and A. Vichi, Carving out OPE space and precise $O(2)$ model critical exponents, J. High Energy Phys. 06 (2020) 142.
[86] F. Kos, D. Poland, and D. Simmons-Duffin, Bootstrapping the $O(N)$ vector models, J. High Energy Phys. 06 (2014) 091.
[87] F. Ihssen, F. R. Sattler, and N. Wink, Numerical RG-time integration of the effective potential: Analysis and Benchmark, Phys. Rev. D **107**, 114009 (2023).
[88] J. W. Thomas, *Numerical Partial Differential Equations: Conservation Laws and Elliptic Equations* (Springer, New York, 1999).
[89] N. Wink, Towards the spectral properties and phase structure of QCD., Ph.D. thesis, University of Heidelberg, ITP, 2020.